Int. J. Heat Mass Transfer. Vol. 25, No. 2, pp. 175–186, 1982
Printed in Great Britain

0017-9310/82/020175-12 $03.00/0

COMBINED FORCED–FREE LAMINAR CONVECTION IN THE ENTRY REGION OF A VERTICAL ANNULUS WITH A ROTATING INNER CYLINDER

M. A. I. EL-SHAARAWI and A. SARHAN
Mechanical Engineering Department, Alazhar University,
Nasr City, Cairo, Egypt

(*Received* 7 *January* 1981 *and in revised form* 8 *June* 1981)

Abstract—Numerical results of a finite difference scheme are presented for the developing combined forced-free laminar boundary layer flow in a vertical concentric annulus with a rotating inner cylinder. The effect of a superimposed aiding or opposing free convection on the developing tangential velocity profiles is investigated for a fluid with $Pr = 0.7$ in an annulus of radius ratio 0.9 over the ranges of $-300 \leqslant Gr/Re \leqslant 800$ and $0.2 \leqslant Re^2/Ta \leqslant 10$. The effects of a rotating inner cylinder on the hydrodynamic development length, critical distance at which the axial velocity gradient normal to the wall vanishes and heat transfer parameters are also considered.

NOMENCLATURE

b, annular gap width, $(r_2 - r_1)$;
c, specific heat of fluid at constant pressure;
D, hydraulic diameter of annulus, $2b$;
g, gravitational body force per unit mass;
Gr, Grashof number, $g\beta(t_w - t_0)D^3/\nu^2$;
h, local heat transfer coefficient based on area of heated surface,
$$-k\frac{\partial t}{\partial r}\bigg|_{\text{wall}}\bigg/(t_m - t_w);$$
k, thermal conductivity of fluid;
n, number of radial increments in the numerical mesh network;
N, annulus radius ratio, r_1/r_2;
Nu, local Nusselt number, hD/k;
p, pressure of fluid at any point;
p_0, pressure of fluid at annulus entrance;
p_s, hydrostatic pressure, $\mp \rho_0 g z$;
p', pressure defect at any point, $p - p_s$;
P, dimensionless pressure defect at any point, $(p' - p_0)/\rho_0 u_0^2$;
Pr, Prandtl number, $\mu c/k$;
r, radial coordinate;
r_1, inner radius;
r_2, outer radius;
R, dimensionless radial coordinate, r/r_2;
Re, Reynolds number, $u_0 D/\nu$;
t, fluid temperature;
t_m, mixing cup temperature over any cross-section,
$$\int_{r_1}^{r_2} utr\,\mathrm{d}r \bigg/ \int_{r_1}^{r_2} ur\,\mathrm{d}r;$$
t_0, fluid temperature at annulus entrance;
t_w, isothermal temperature of heated wall;
T, dimensionless temperature, $(t - t_0)/(t_w - t_0)$;
T_m, dimensionless mixing cup temperature, $(t_m - t_0)/(t_w - t_0)$;
Ta, Taylor number, $2\Omega^2 r_1^2 b^3/\nu^2(r_1 + r_2)$;
u, axial velocity;
u_0, entrance axial velocity, $\int_{r_1}^{r_2} ur\,\mathrm{d}r \Big/ \int_{r_1}^{r_2} r\,\mathrm{d}r$;
U, dimensionless axial velocity, u/u_0;
v, radial velocity;
V, dimensionless radial velocity, vr_2/ν;
w, tangential velocity;
W, dimensionless tangential velocity, $w/\Omega r_1$;
z, axial coordinate;
Z, dimensionless axial coordinate, $2z(1 - N)/r_2 Re$;
Z_0, dimensionless hydrodynamic development length;
Z_r, dimensionless axial distance at which the gradient of the axial velocity component normal to the wall vanishes.

Greek symbols

β, volumetric coefficient of thermal expansion;
ρ, fluid density, $\rho_0[1 - \beta(t - t_0)]$;
ρ_0, fluid density at the entrance temperature;
μ, dynamic viscosity of fluid;
ν, kinematic viscosity of fluid, μ/ρ_0;
δ_θ, tangential boundary layer displacement thickness,
$$\int_{r_1}^{r_2} w\,\mathrm{d}r/\Omega r_1;$$
δ_θ^*, dimensionless tangential boundary layer displacement thickness, δ_θ/b;
Ω, angular velocity of inner cylinder.

1. INTRODUCTION

SINCE the famous paper of G. I. Taylor [1], there has been increasing interest in knowing the variables which control the laminar flow behaviour and the onset of hydrodynamic instability in concentric annuli with rotating inner walls. Investigating such a problem leads to a basic understanding of fluid flow through the gap between rotating and stationary machine parts, such that in electric motors, journal bearings, chemical mixing or drying machinery, gas or oil exploration drills etc.

Few papers in the literature [2–8] have dealt with tangentially developing laminar flows and/or transition to vorticular motion in the entrance region of concentric annuli with rotating inner walls. The main aim of these papers was the determination of the axial growth of the tangential boundary layer displacement thickness δ_θ. According to the unique stability criterion available to date for tangentially developing flows [2, 3], knowledge of the axial growth of δ_θ is essential to locate the axial position of the point of origin of hydrodynamic instability.

In fact, these entry region investigations have been developed under the assumption of temperature-independent fluid properties. However, high heating or cooling rates may cause significant changes in fluid properties and the classical assumption of constant physical properties may lead to considerable errors in predicting the flow behaviour and both the power required to pump the fluid and the heat transfer characteristics.

Of particular interest to the present investigation is the variation of fluid density with temperature. A change in fluid density causes a change in the gravitational body force on a volume of the fluid. At low Reynolds number gravitational body forces play an important role in determining the flow regime. Under certain circumstances body forces created under the action of temperature-dependent fluid density may change a forced laminar flow to the so-called combined forced–free, or mixed convection laminar flow. On the other hand, changes in fluid density resulting from the presence of radial temperature gradients, due to heating or cooling one or both of the annulus boundaries, affect the stability of a Couette flow between two rotating concentric cylinders [9]. Also, variations with temperature of fluid density may create distortions affecting the stability of a streamline axial flow and cause transition to an unsteady flow at Reynolds numbers much lower than those with isothermal flow [10].

The present study is an attempt to investigate the free convection effects on the developing laminar upward or downward flow in a vertical annulus with a rotating inner cylinder. Two thermal boundary conditions are considered; namely, case (I) in which the inner rotating wall is isothermal while the outer stationary wall is adiabatic, and case (O) in which the outer wall is isothermal while the inner wall is adiabatic.

2. GOVERNING EQUATIONS

Assuming steady, axisymmetric, laminar flow of an incompressible Newtonian fluid, with no internal heat generation, with constant physical properties except the density which only varies in the gravitational body force term according to the Boussinesq approximation, neglecting viscous dissipation and axial conduction of heat, assuming $Re \gg 0$, and applying the Prandtl boundary layer assumptions [2], the equations governing the combined forced–free fluid motion and heat transfer in the entrance region of a vertical annulus with a rotating inner cylinder are as follows:

$$\frac{\partial(rv)}{\partial r} + \frac{\partial(ru)}{\partial z} = 0\,, \tag{1}$$

$$\rho_0 \frac{w^2}{r} = \frac{\partial p}{\partial r}\,, \tag{2}$$

$$\rho_0\left(v\frac{\partial w}{\partial r} + u\frac{\partial w}{\partial z}\right) = \mu\frac{\partial}{\partial r}\left[\frac{1}{r}\frac{\partial}{\partial r}(rw)\right], \tag{3}$$

$$\rho_0\left(v\frac{\partial u}{\partial r} + u\frac{\partial u}{\partial z}\right) = -\frac{\partial p}{\partial z} \mp \rho_0 g[1 - \beta(t - t_0)] + \frac{\mu}{r}\frac{\partial}{\partial r}\left(r\frac{\partial u}{\partial r}\right), \tag{4}$$

$$\rho_0 c\left(v\frac{\partial t}{\partial r} + u\frac{\partial t}{\partial z}\right) = \frac{k}{r}\frac{\partial}{\partial r}\left(r\frac{\partial t}{\partial r}\right). \tag{5}$$

The minus and plus signs in the gravitational term of equation (4) apply respectively to upward and downward flows, taking into consideration that the body force acts in the negative z-direction in case of an upward flow and vice versa in case of a downward flow.

Dissociating the pressure into the usual two components, i.e.

$$p = p' + p_s = p' \mp \rho_0 g z, \tag{6}$$

in which the minus and plus signs apply respectively to upward and downward flows, equations (2) and (4) can be written as follows

$$\rho_0 \frac{w^2}{r} = \frac{\partial p'}{\partial r}\,, \tag{7}$$

$$\rho_0\left(v\frac{\partial u}{\partial r} + u\frac{\partial u}{\partial z}\right) = -\frac{\partial p'}{\partial z} \pm \rho_0 g\beta(t - t_0) + \frac{\mu}{r}\frac{\partial}{\partial r}\left(r\frac{\partial u}{\partial r}\right). \tag{8}$$

Using the dimensionless parameters given in the nomenclature, equations (1), (3), (5), (7) and (8) can be replaced by the following dimensionless forms:

$$\frac{\partial V}{\partial R} + \frac{V}{R} + \frac{\partial U}{\partial Z} = 0\,, \tag{9}$$

$$\frac{W^2}{R} = \frac{(1-N)}{2(1+N)}\frac{Re^2}{Ta}\frac{\partial P}{\partial R}\,, \tag{10}$$

$$V\frac{\partial W}{\partial R} + U\frac{\partial W}{\partial Z} = \frac{\partial^2 W}{\partial R^2} + \frac{1}{R}\frac{\partial W}{\partial R} - \frac{W}{R^2}\,, \tag{11}$$

$$V\frac{\partial U}{\partial R}+U\frac{\partial U}{\partial Z}=-\frac{\partial P}{\partial Z}\pm\frac{Gr}{Re}\frac{T}{4(1-N)^2}+\frac{\partial^2 U}{\partial R^2}+\frac{1}{R}\frac{\partial U}{\partial R}, \quad (12)$$

$$V\frac{\partial T}{\partial R}+U\frac{\partial T}{\partial Z}=\frac{1}{Pr}\left(\frac{\partial^2 T}{\partial R^2}+\frac{1}{R}\frac{\partial T}{\partial R}\right). \quad (13)$$

The five coupled equations (9)–(13) are subject to the following boundary conditions:

for $Z \geqslant 0$ and $R = N, U = V = 0, W = 1$ and $T = 1$ for case (I) or $\partial T/\partial R = 0$ for case (O);

for $Z \geqslant 0$ and $R = 1, U = V = W = 0$ and $\partial T/\partial R = 0$ for case (I) or $T = 1$ for case (O);

for $Z = 0$ and $N < R < 1, V = W = T = P = 0$ and $U = 1$. (14)

Using the boundary conditions (14), the continuity equation (9) can be written in the following integral form:

$$\int_N^1 RU\,dR=\frac{1}{2}(1-N^2). \quad (15)$$

It is worth noting that the above mathematical model which governs the present mixed convection case includes the extra similarity parameter Gr/Re beside those similarity parameters describing the purely forced convection case [7, 8].

3. NUMERICAL METHOD OF SOLUTION

Considering the mesh network of Fig. 1, and by an extension of the work of [7], equations (9)–(13) and equation (15) can be written in the following finite difference forms:

$$\frac{V_{i+1,j+1}-V_{i,j+1}}{\Delta R}+\frac{V_{i+1,j+1}+V_{i,j+1}}{2[N+(i-1/2)\Delta R]}+\frac{U_{i+1,j+1}+U_{i,j+1}-U_{i+1,j}-U_{i,j}}{2\Delta Z}=0, \quad (16)$$

$$\frac{W_{i,j}W_{i,j+1}}{N+(i-1)\Delta R}=\frac{(1-N)}{2(1+N)}\times\frac{Re^2}{Ta}\frac{P_{i,j+1}-P_{i-1,j+1}}{\Delta R}, \quad (17)$$

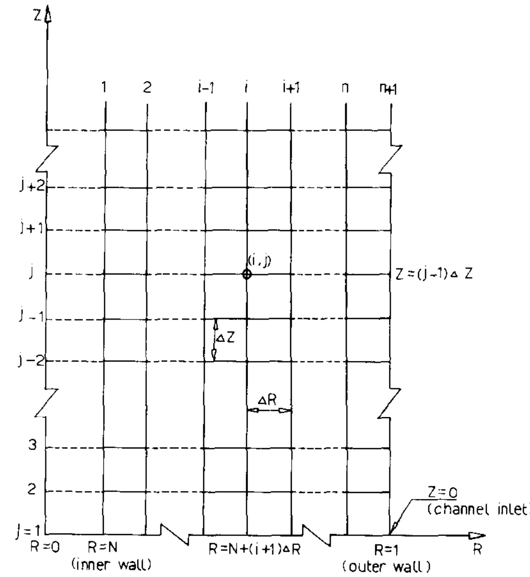

FIG. 1. Mesh network for finite difference representation.

$$V_{i,j}\frac{U_{i+1,j+1}-U_{i-1,j+1}}{2\Delta R}+U_{i,j}\frac{U_{i,j+1}-U_{i,j}}{\Delta Z}=\frac{P_{i,j}-P_{i,j+1}}{\Delta Z}+\frac{Gr}{Re}\frac{T_{i,j+1}}{4(1-N)^2}+\frac{U_{i+1,j+1}-2U_{i,j+1}+U_{i-1,j+1}}{(\Delta R)^2}+\frac{1}{N+(i-1)\Delta R}\frac{U_{i+1,j+1}-U_{i-1,j+1}}{2\Delta R}, \quad (19)$$

$$V_{i,j}\frac{T_{i+1,j+1}-T_{i-1,j+1}}{2\Delta R}+U_{i,j}\frac{T_{i,j+1}-T_{i,j}}{\Delta Z}=\frac{1}{Pr}\left(\frac{T_{i+1,j+1}-2T_{i,j+1}}{(\Delta R)^2}+\frac{T_{i-1,j+1}}{(\Delta R)^2}+\frac{1}{N+(i-1)\Delta R}\frac{T_{i+1,j+1}-T_{i-1,j+1}}{2\Delta R}\right), \quad (20)$$

$$\Delta R\sum_{i=2}^{n}U_{i,j}[N+(i-1)\Delta R]=\frac{1}{2}(1-N^2). \quad (21)$$

$$V_{i,j}\frac{W_{i+1,j+1}+W_{i+1,j}-W_{i-1,j}-W_{i-1,j+1}}{4\Delta R}+U_{i,j}\frac{W_{i,j+1}-W_{i,j}}{\Delta Z}=\frac{W_{i+1,j+1}+W_{i+1,j}-2W_{i,j+1}-2W_{i,j}+W_{i-1,j+1}+W_{i-1,j}}{2(\Delta R)^2}+\frac{1}{N+(i-1)\Delta R}\times\frac{W_{i+1,j+1}+W_{i+1,j}-W_{i-1,j}-W_{i-1,j+1}}{4\Delta R}-\frac{W_{i,j+1}+W_{i,j}}{2[N+(i-1)\Delta R]^2}, \quad (18)$$

In the above finite difference equations the variables with subscript $j+1$ represent the unknowns and those with subscript j are knowns. The numerical solution of these equations is obtained by first selecting values of the parameters Re^2/Ta, Gr/Re and Pr. Then, starting with $j = 1$ (entrance cross-section) and applying equation (18) for $i = 2, 3, \ldots, n$ yields $(n - 1)$ simultaneous linear algebraic equations which when solved by Thomas' method [11] give the unknown values of W's at all points of the second cross-section. Similarly, using equation (20) the unknown values of T's at all points of the second cross-section ($j = 2$) are obtained. Now, applying (17) with $i = 2, 3, \ldots, n+1$ and (19) with $i = 2, 3, \ldots, n$ and (21) to the entire cross-section, we get $2n$ equations which when solved, by means of a special form of the Gauss–Jordan elimination scheme [12], give the unknown values of U's and P's at all points of the second cross-section. Using the computed values of U's and applying (16) we get the unknown values of V's at the grid points of the second cross-section. Repeating this procedure, we can advance along the annulus until the flow becomes fully developed.

4. CONVERGENCE OF THE FINITE DIFFERENCE SCHEME

The numerical solution of the finite difference equations (16)–(20) must converge to the exact solution of the original partial differential equations (9)–(13) in the limit when the numerical grid spacings tend to zero. To ensure such an essential requirement, the finite difference equations must be consistent representations of the original differential equations (i.e. truncation errors tend to zero as the numerical mesh sizes tend to zero) and stable (i.e. round-off errors do not grow as the computations proceed in the marching direction). Details concerning consistency and stability and theories relating them with convergence may be found in [12].

Following the procedures described in [12, 15] and expanding each term in the finite difference equations (16)–(20) by a Taylor series, it could easily be proved that the truncation errors, resulting from the approximation of each of the differential equations (9)–(13) by the finite difference equations (16)–(20), respectively, vanish as the mesh sizes tend to zero. This means that the finite difference equations (16)–(20) are consistent representations of equations (9)–(13).

Also, according to the theories summarized in [12, 15], the numerical stability can be examined by introducing small perturbations (denoted hereinafter by U', V', W', P' and T') into the finite difference equations and checking whether or not such perturbations amplify as the computation proceeds in the marching direction. It is noteworthy that the finite difference equations are linearized by assuming that, where the product of two unknowns (with subscript $j+1$) occurs, one of them is given approximately by its value at the previous axial step (with subscript j). This implies that one of these unknowns is considered as a constant throughout an axial step. Thus, the coefficient $W_{i,j}$ on the left hand side of equation (17) and also the coefficients $U_{i,j}$ and $V_{i,j}$ which are multiplied by the finite difference representations of the derivatives $\partial W/\partial R$, $\partial W/\partial Z$, $\partial U/\partial R$, $\partial U/\partial Z$, $\partial T/\partial R$ and $\partial T/\partial Z$ on the left hand sides of equations (18)–(20) may be regarded as being constants throughout an axial step. Therefore, taking into account the constancy of such coefficients throughout an axial step, the insertion of the new variables $U + U'$, $V + V'$, $W + W'$, $P + P'$ and $T + T'$ into the finite difference equations (16)–(20) leads to five other equations which are identical in form to the finite difference equations (i.e. these resulting five equations can be obtained by replacing each variable in the finite difference equations, except the previously mentioned constant coefficients, by its corresponding perturbation). These resulting five equations govern the behaviour of the small perturbations which represent the round-off or similar errors, i.e. they give the relationships between the values of such numerical errors at a column (e.g. $j+1$) and the corresponding values of these errors at the previous axial step (i.e. column j). Moreover, according to these stability theories summarized in [12, 15], a general term of a particular numerical error (i.e. a primed variable) at any point (R, Z) is a product of two functions; the first of these is an exponential function of Z only which represents the amplitude of the error at the particular point under consideration while the second is an exponential function of R only, containing all the existing harmonics. A typical form of this general term at any column (say for example j) is $f(Z)\,e^{IqR}$, where I denotes the square root of -1, q is any real number representing the frequency of any existing harmonic, and $f(Z)$ is an exponential function of Z only representing the amplitude of the error at that particular column.

Now using such a typical form for all the perturbations, we have $U'_{i,j} = f_1(Z)\,e^{IqR}$, $V'_{i,j} = f_2(Z)\,e^{IqR}$, $W'_{i,j} = f_3(Z)\,e^{IqR}$, $P'_{i,j} = f_4(Z)\,e^{IqR}$, and $T'_{i,j} = f_5(Z)\,e^{IqR}$, where each f is again an exponential function of Z only representing the amplitude of the corresponding perturbation. Substituting these sinusoidal representations of the perturbations in the previously-mentioned resulting five equations which govern the behaviour of the round-off or similar errors, i.e. equations (16)–(20) after replacing each variable by its corresponding perturbation, leads to the following five simultaneous equations:

$$
\begin{aligned}
f_1(Z + \Delta Z) &= c_1 f_1(Z) + c_2 f_4(Z) + c_3 f_5(Z),\\
f_2(Z + \Delta Z) &= c_4 f_1(Z) + c_5 f_4(Z) + c_6 f_5(Z),\\
f_3(Z + \Delta Z) &= c_7 f_3(Z),\\
f_4(Z + \Delta Z) &= c_7 f_4(Z),\\
f_5(Z + \Delta Z) &= c_8 f_5(Z),
\end{aligned}
\qquad (22)
$$

in which

$$c_1 = 1/(1 - BS),$$

$$c_2 = (1 - c_7)/(U - UBS),$$

$$c_3 = \frac{Gr}{4(1 - N)^2 Re} \frac{S(\Delta R)^2}{1 - BS} c_8,$$

$$c_4 = -1 \Bigg/ \left[2\left(\frac{\Delta Z}{\Delta R}\right)\left(\frac{A - 1}{A + 1} + \frac{\Delta R}{2R_{i+1/2}}\right)\left(\frac{1}{BS} - 1\right) \right],$$

$$c_5 = c_4 c_2 \left(\frac{1}{BS} - 1\right),$$

$$c_6 = c_3 c_5 / c_2,$$

$$c_7 = \frac{2 - S[(\Delta R/R_i)^2 - B]}{2 + S[(\Delta R/R_i)^2 - B]},$$

$$c_8 = \frac{Pr}{Pr - S[B + IV\Delta R(1 - Pr)\sin q\Delta R]},$$

$$S = \frac{\Delta Z}{U(\Delta R)^2},$$

$$A = e^{IQ\Delta R},$$

$$B = 2(\cos q\Delta R - 1) - I\left(V\Delta R - \frac{\Delta R}{R_i}\right)\sin q\Delta R.$$

The above equations can be expressed in the following matrix–vector notations

$$\bar{F}(Z + \Delta Z) = G\bar{F}(Z),$$

where $\bar{F}(Z + \Delta Z)$ and $\bar{F}(Z)$ are the column vectors whose components represent the amplitudes of the individual error components corresponding to the various dependent variables at $(Z + \Delta Z)$ and Z, respectively, while G is a complex matrix of dimension 5×5, known as the amplification matrix.

Again, according to the theories summarized in [12, 15], for numerical stability, each eigenvalue of the amplification matrix **G** must not exceed unity in modulus. Denoting the five eigenvalues of **G** by $\mathscr{L}_1$, $\mathscr{L}_2$, $\mathscr{L}_3$, $\mathscr{L}_4$ and $\mathscr{L}_5$, then we have

$$\mathscr{L}_1 = 1/(1 - BS), \quad \mathscr{L}_2 = 0,$$

$$\mathscr{L}_3 = \mathscr{L}_4 = c_7, \quad \mathscr{L}_5 = c_8.$$

Denoting the moduli of these eigenvalues by $\mathscr{L}'_1$, $\mathscr{L}'_2$, $\mathscr{L}'_3$, $\mathscr{L}'_4$ and $\mathscr{L}'_5$ respectively, it can easily be proved that

$$\mathscr{L}'_1 = \sqrt{1/(1 + 4E_1 + 4E_1^2 + E_2^2)},$$

$$\mathscr{L}'_2 = 0,$$

$$\mathscr{L}'_3 = \mathscr{L}'_4 = \sqrt{\frac{1 - 2E_3 + E_3^2 + (E_2/2)^2}{1 + 2E_3 + E_3^2 + (E_2/2)^2}},$$

$$\mathscr{L}'_5 = \sqrt{1/[1 + (4E_1/Pr) + (2E_1/Pr)^2 + E_4^2]},$$

where

$$E_1 = -S(\cos q\Delta R - 1),$$

$$E_2 = S(V\Delta R - \Delta R/R_i)\sin q\Delta R,$$

$$E_3 = -S\left(\cos q\Delta R - 1 - \frac{\Delta R^2}{2R_i^2}\right),$$

$$E_4 = S\left(V\Delta R - \frac{\Delta R}{R_i Pr}\right)\sin q\Delta R.$$

In the above-mentioned expressions it is to be noted that the squared quantities are always positive and that, since $\cos q\Delta R$ ranges from -1 to 1, the quantities E_1 and E_3 are also positive if S is positive. However, S is positive if U is positive. Therefore, in such a case (U positive), each of the above given moduli is, for all mesh sizes, less than unity. Hence, the finite difference equations (16)–(20) are stable for all mesh sizes as long as the downstream axial velocity is positive, i.e. as long as no flow reversals occur within the domain of solution.

It is worth mentioning here that the left-hand side of equation (17) was given in [7] as $W_{i,j+1}^2/R_i$. Even though such a representation for W^2/R at the grid point $(i, j + 1)$ is exact and would not affect the previously mentioned method of solution, it does not, however, guarantee numerical stability. This is because, in this case and after neglecting the 2nd-order terms of the perturbations, equation (22) would take the form

$$f_4(Z + \Delta Z) = c_7 f_4(z)\, W_{i,j+1}/W_{i,j},$$

while the other four equations, which govern the behaviour of errors, would remain unchanged. Hence, in this case, one of the eigenvalues of the amplification matrix would become $\mathscr{L}_4 = c_7 W_{i,j+1}/W_{i,j}$ while the other four eigenvalues remain the same as previously given. Since $W_{i,j+1}/W_{i,j}$ is normally greater than unity for tangentially developing flows, hence $\mathscr{L}_4$ is not unconditionally guaranteed, in this case, to be less than unity in modulus and thus numerical stability may not be secured as was inaccurately stated in [7, 8].

5. RESULTS AND DISCUSSION

The special case of $Gr/Re = 0$ (i.e. pure forced convection with constant physical properties) has been treated in [7, 8] and it was stated in [8] that a laminar solution would not exist over the entire development length for values of the parameter $Re^2/Ta < 1$. The present approximate representation of W^2 at the grid point $(i, j + 1)$ by the linearized expression $W_{i,j}W_{i,j+1}$ in the finite difference equation (17), rather than the exact representation $W_{i,j+1}^2$ used in [7], has been successful in obtaining converged laminar numerical solutions over the entire development length at values of the parameter $Re^2/Ta < 1$. However, at sufficiently low values of Re^2/Ta, and even though the condition for numerical stability (i.e. U is non-negative within the domain of solution) is satisfied, a laminar numerical solution could only be obtained up to a certain axial distance from the annulus entrance, after which divergence from the laminar solution occurs. The point at which the solution starts to diverge always moves toward the annulus entrance as the value of the parameter Re^2/Ta further decreases. Such a solution divergence appears as the radial velocity component starts to increase instead of decaying as in the laminar flow solution. Since the condition for numerical stability is satisfied, one may say that such a phenomenon (of a non-existent laminar solution which occurs after a certain axial length, at sufficiently low values of Re^2/Ta) is not linked with a numerical instability but rather it is a physical instability. It is also important to mention that Schlichting [16] explained the physical reasons due which one "must not expect" laminar solutions to be available "for arbitrary large $\Omega r_1/u_0''$, i.e. for sufficiently low values of Re^2/Ta.

On the other hand, the special case of $Re^2/Ta = \infty$ (i.e. stationary walls) has been treated in [13] and it was shown that, at large absolute values of Gr/Re, there exists a possibility of flow reversals near the heated boundary when the free convection opposes the forced flow (i.e. negative values of Gr/Re) while such a flow reversal may occur near the insulated wall if the free convection is aiding the forced flow (i.e. positive values of Gr/Re). This prediction can physically be attributed to the fact that, when the free convection aids the forced flow, the fluid accelerates near the heated boundary and, due to the continuity principle, decelerates near the opposite insulated wall, and vice versa when the free convection opposes the forced flow. It should be emphasized that such flow reversals would be expected to exist, at sufficiently large values of Gr/Re, regardless of the shape of the inlet velocity profile. However, the axial distance at which such a flow reversal may occur would be dependent on the shape of the inlet velocity profile. Also, it was shown in [13] that before the occurrence of a flow reversal, the velocity gradient normal to the wall, near which the flow reversal occurs, vanishes ($\partial U/\partial R|_{\text{wall}} = 0$) and the critical distance Z_r, at which the velocity gradient vanishes, was computed for each chosen value of the parameter Gr/Re.

With a superimposed free convection (i.e. $Gr/Re \neq 0$) and a rotatable inner cylinder (i.e. $Re^2/Ta \neq \infty$), the present computations have confirmed the phenomenon of nonexistent laminar solutions, after certain axial distances from the entrance at sufficiently low values of the parameter Re^2/Ta, even though the condition for numerical stability is satisfied. Moreover, it has been found, as can be seen from Table 1, that either in case (I) with an opposing free convection (i.e. negative values of Gr/Re) or in case (O) with an aiding free convection (i.e. positive values of Gr/Re), increasing the absolute value of Gr/Re (i.e. increasing the free convection effect) causes an increase in the value of the parameter Re^2/Ta at which such a phenomenon (i.e. divergence from laminar solution before the flow reaches full development, even though the condition for numerical stability is satisfied) occurs. This can physically be attributed to the fact that in both cases [i.e. case (I) with an opposing free convection or case (O) with an aiding free convection] the free convection causes a decrease in the axial velocity component near the rotating inner wall; a decrease in the axial velocity component is known to have a destabilizing effect [14] and hence transition from the laminar regime is expected to occur at low values of Ta (i.e., high values of Re^2/Ta). Again, this latter prediction, beside the fact that the condition for numerical stability has not been violated until that cross-section at which the solution starts to diverge, may confirm that this phenomenon is not linked with a numerical instability but rather it is a physical instability.

Effect of a rotating inner cylinder on the hydrodynamic development length Z_0 and the critical distance Z_r

Table 1 gives, for an annulus of $N = 0.9$ with $Pr = 0.7$, the critical distance Z_r, at which the gradient of the axial velocity component normal to the wall vanishes, and the hydrodynamic development length Z_0, defined as the axial distance from the entrance required for the flow to become within $\pm 0.5\%$ axially fully developed [13]. It is clear from this table that, in the absence of free convection (i.e. $Gr/Re = 0$), the inner cylinder rotation increases the hydrodynamic development length significantly in comparison with the case of flow in a stationary annulus (i.e. $Re^2/Ta = \infty$). This increase in the hydrodynamic development length is dependent on the value of the parameter Re^2/Ta and could reach more than 1000% for $Re^2/Ta = 0.2$. This shows how the mechanism of axial velocity development becomes very slow due to the inner cylinder rotation in comparison with the stationary walls case. This prediction is in a qualitative agreement with the results of the integral momentum analysis of Astill and Chung [6] which have showed that the closing length of the two axial boundary layers in an annulus increases as the value of the parameter Re^2/Ta decreases.

With a superimposed free convection (i.e. $Gr/Re \neq 0$), Table 1 shows that for a given value of Gr/Re the effect of the inner cylinder rotation on either the hydrodynamic development length or the critical distance Z_r, if any, depends on whether the free convection is aiding or opposing the forced flow and on the thermal boundary conditions. With an aiding free convection (i.e. positive values of Gr/Re), increasing the inner cylinder rotational speed (i.e. decreasing the value of Re^2/Ta at a given value of Gr/Re) increases Z_0 and decreases Z_r in case (I) and vice versa in case (O). On the other hand, if the free convection opposes the forced flow (i.e. negative values of Gr/Re), increasing the inner cylinder rotational speed decreases Z_0 and increases Z_r in case (I) and vice versa in case (O). These effects could be attributed to the fact that the inner cylinder rotation has, in all cases, the effect of increasing the axial velocity component near the rotating inner cylinder [6, 7] (i.e. the developing axial velocity profiles become more skewed inward as shown in Fig. 2). However, while the superimposed aiding and opposing free convections have a similar

Table 1. Critical distance Z_r and the hydrodynamic development length Z_0 ($N = 0.9$, $Pr = 0.7$)

Gr/Re	$Re^2/Ta = \infty$ $Z_r x 10^4$	$Re^2/Ta = \infty$ $Z_0 x 10^2$	$Re^2/Ta = 10$ $Z_r x 10^4$	$Re^2/Ta = 10$ $Z_0 x 10^2$	$Re^2/Ta = 1$ $Z_r x 10^4$	$Re^2/Ta = 1$ $Z_0 x 10^2$	$Re^2/Ta = 0.5$ $Z_r x 10^4$	$Re^2/Ta = 0.5$ $Z_0 x 10^2$	$Re^2/Ta = 0.3$ $Z_r x 10^4$	$Re^2/Ta = 0.3$ $Z_0 x 10^2$	$Re^2/Ta = 0.2$ $Z_r x 10^4$	$Re^2/Ta = 0.2$ $Z_0 x 10^2$
					Thermal boundary condition (O)							
−300	3.33	1.315	3.32	NI	3.25	NI	3.12	NI	3.00	NI		
−200	NFR	1.203	NFR	1.220	NFR	1.288	NFR	1.307	NFR	1.314	NFR	1.330
−100	NFR	1.001	NFR	1.002	NFR	1.009	NFR	1.028	NFR	1.032	NFR	1.040
0	NFR	0.059	NFR	0.105	NFR	0.480	NFR	0.570	NFR	0.600	NFR	0.610
100	NFR	0.840	NFR	0.835	NFR	0.816	NFR	0.802	NFR	0.790	NFR	0.781
200	NFR	1.042	NFR	1.038	NFR	1.010	NFR	1.002	NFR	1.000	NFR	SD
400	NFR	1.260	NFR	1.242	NFR	1.140	NFR	1.125	NFR	SD		
500	NFR	1.332	NFR	1.327	NFR	1.264	NFR	SD				
700	7.80	1.432	7.88	1.421	8.40	NI	NFR	SD				
800	6.80	1.481	6.80	NI	6.70	NI	NFR	SD				
					Thermal boundary condition (I)							
−300	3.30	1.562	3.50	NI	NFR	SD						
−200	NFR	1.396	NFR	1.381	NFR	1.356	NFR	1.350	NFR	SD		
−100	NFR	1.118	NFR	1.117	NFR	1.116	NFR	1.115	NFR	1.110	NFR	1.102
100	NFR	0.878	NFR	0.900	NFR	0.993	NFR	1.019	NFR	1.020	NFR	1.026
200	NFR	1.092	NFR	1.135	NFR	1.220	NFR	1.252	NFR	1.258	NFR	1.263
400	NFR	1.312	NFR	1.335	NFR	1.420	NFR	1.440	NFR	1.450	NFR	1.456
500	NFR	1.387	NFR	1.407	NFR	1.476	NFR	1.490	NFR	1.500	NFR	1.510
700	9.40	1.514	9.37	1.523	9.08	1.561	8.80	1.565	8.60	1.570	8.40	1.577
800	7.66	1.566	7.65	1.572	7.60	1.600	7.58	NI	7.30	NI		
900	6.80	NI	6.79	NI	6.78	NI	6.75	NI	6.70	NI		

NFR = neither flow reversal nor zero velocity gradient normal to the wall occur.

NI = numerical instability occurs before the flow reaches full development due to the presence of flow reversals within the domain of solution.

SD = solution divergence occurs before the flow reaches full development, even though the condition for numerical stability is satisfied.

effect in cases (I) and (O), respectively, they cause a decrease in the axial velocity component near the rotating inner cylinder in cases (O) and (I), respectively [13]. Thus, both the inner cylinder rotation and the aiding free convection of case (I) or the opposing free convection of case (O) have similar effects on the developing axial velocity profiles. On the other hand, the aiding free convection of case (O) or the opposing free convection of case (I) counter acts the effect of the inner cylinder rotation on the developing axial velocity profiles. Therefore, for a given value of Gr/Re and in either case (I) with an aiding free convection or case (O) with an opposing free convection, the developing axial velocity profiles deviate increasingly from the corresponding isothermal developing profiles by decreasing the value of the parameter Re^2/Ta. On the other hand, such a deviation decreases in either case (I) with an opposing free convection or case (O) with an aiding free convection by increasing the inner cylinder rotational speed. Hence, the axial distance required for the axial velocity profiles to recover and approach the fully developed isothermal velocity profile increases in the former two cases and decreases in the latter two cases, but the critical distance Z_r, if any, is affected in a reversed manner. This is because the more is the deviation of the developing axial velocity profiles from the corresponding developing isothermal velocity profiles the more is the possibility of having a flow reversal

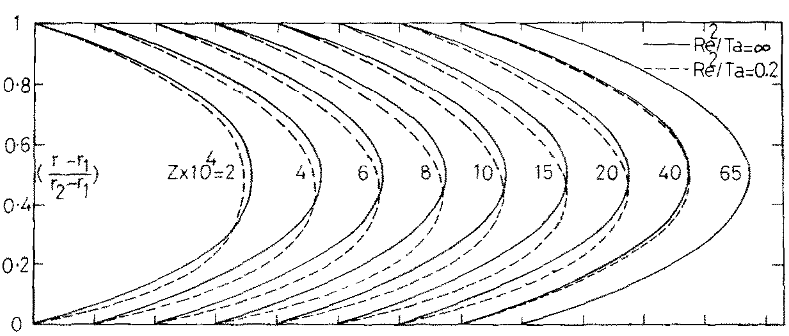

FIG. 2. Effect of inner cylinder rotation on the developing axial velocity profiles, $N = 0.9$; $Gr/Re = 0$.

and hence the shorter is the axial distance (from the entrance) at which such a flow reversal may occur. On the other hand, if there is no flow reversals, the more is the deviation (of the developing axial velocity profiles from the corresponding developing isothermal velocity profiles) the longer is the axial distance (from the entrance) required for such profiles to recover and approach the isothermal fully developed axial velocity profile.

Effect of a superimposed free convection on the developing tangential velocity profiles and δ_θ

In the absence of free convection, it is known [2–7] that, provided the flow remains laminar and vortices are not generated, the rate of rotation of the inner cylinder has a slight effect on the developing tangential velocity profiles, and hence δ_θ. In the presence of a superimposed free convection, the present computations have also confirmed this conclusion. In other words, at a given value of Gr/Re, the parameter Re^2/Ta has a slight effect on the developing tangential velocity profiles, and hence δ_θ. To show such a slight effect more clearly, values of δ_θ^*, corresponding to some selected values of the parameter Gr/Re, are presented in Table 2 for an annulus of radius ratio 0.9 at various axial positions for two values of the parameter Re^2/Ta (0.2 and 10).

On the other hand, for a given value of Re^2/Ta, the parameter Gr/Re and the thermal boundary conditions have significant effects on the developing tangential velocity profiles, and hence δ_θ. Figures 3 and 4 represent, for thermal boundary conditions (I) and (O) respectively, the developing tangential velocity distribution W corresponding to a given value of the parameter Re^2/Ta for various selected values of the parameter Gr/Re. However, in order to show the effect of the thermal boundary conditions more clearly, the developing tangential velocity profiles given in Fig. 5 are obtained by cross-plotting in Figs. 3 and 4. Figures 6 and 7 represent, for a given value of the parameter Re^2/Ta, the developing dimensionless tangential boundary layer displacement thickness against the dimensionless axial distance for some selected values of the parameter Gr/Re. It is noticeable from these figures that, near the annulus entrance and until a certain point in the entry region, the superimposed aiding and opposing free convections of cases (I) and (O) respectively delay the development of the tangential velocity component in comparison with the case of pure forced convection (i.e. $Gr/Re = 0$), then further downstream this effect is reversed. Also, in either case (I) with an opposing free convection or case (O) with an aiding free convection, the increase in the absolute

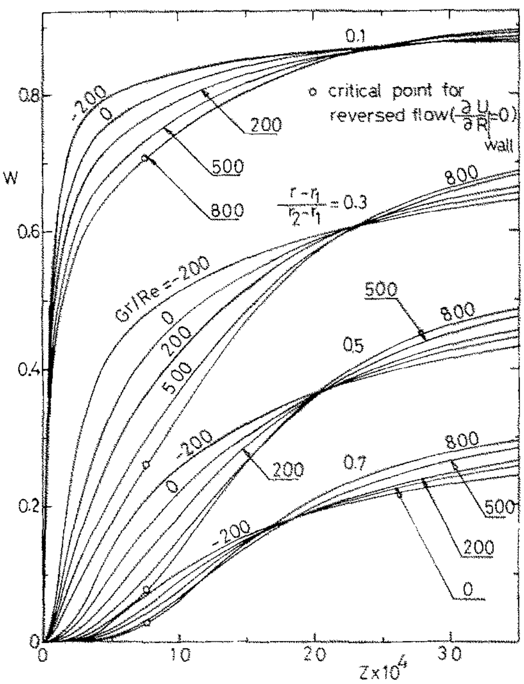

FIG. 3. Tangential velocity development for various values of Gr/Re, $N = 0.9$; $Pr = 0.7$; $Re^2/Ta = 10$; case (I).

Table 2. Effect of the parameter Re^2/Ta on the dimensionless tangential boundary layer displacement thickness ($N = 0.9$, $Pr = 0.7$)

	δ_θ^*									
	Case (O)				Case (I)				Pure forced convection	
	$Gr/Re = 100$		$Gr/Re = -100$		$Gr/Re = 100$		$Gr/Re = -100$		$Gr/Re = 0$	
$Z \times 10^4$	$Re^2/Ta = 10$	$Re^2/Ta = 0.2$	$Re^2/Ta = 10$	$Re^2/Ta = 0.2$	$Re^2/Ta = 10$	$Re^2/Ta = 0.2$	$Re^2/Ta = 10$	$Re^2/Ta = 0.2$	$Re^2/Ta = 10$	$Re^2/Ta = 0.2$
2	0.1815	0.1694	0.1681	0.1599	0.1672	0.1589	0.1862	0.1719	0.1750	0.1650
5	0.2620	0.2491	0.2332	0.2257	0.2342	0.2263	0.2646	0.2510	0.2474	0.2377
10	0.3379	0.3312	0.3118	0.3046	0.3133	0.3059	0.3367	0.3309	0.3244	0.3175
15	0.3839	0.3826	0.3695	0.3642	0.3712	0.3658	0.3822	0.3818	0.3722	0.3721
20	0.4147	0.4172	0.4097	0.4078	0.4114	0.4096	0.4134	0.4165	0.4128	0.4124
30	0.4513	0.4565	0.4561	0.4595	0.4571	0.4610	0.4506	0.4560	0.4544	0.4582
45	0.4751	0.4794	0.4827	0.4879	0.4829	0.4882	0.4746	0.4793	0.4789	0.4838
90	0.4891	0.4895	0.4919	0.4925	0.4917	0.4922	0.4888	0.4893	0.4904	0.4908
240	0.4908	0.4908	0.4908	0.4908	0.4908	0.4908	0.4908	0.4908	0.4908	0.4908

value of the parameter Gr/Re causes an increase in the rate of tangential velocity development until a certain axial distance from the entrance is reached, after which this effect is reversed until the flow becomes fully developed.

In order to interpret the effects of a superimposed free convection on the development of the tangential velocity component, recourse to the mechanisms of transporting the tangential momentum in the entry region is necessary. The tangential momentum is transported in the entry region by two mechanisms; firstly, by the transport created by the radial velocity component and, secondly, by the molecular diffusion due to the viscosity of the fluid. As can be seen from Fig. 8, for an aiding free convection with

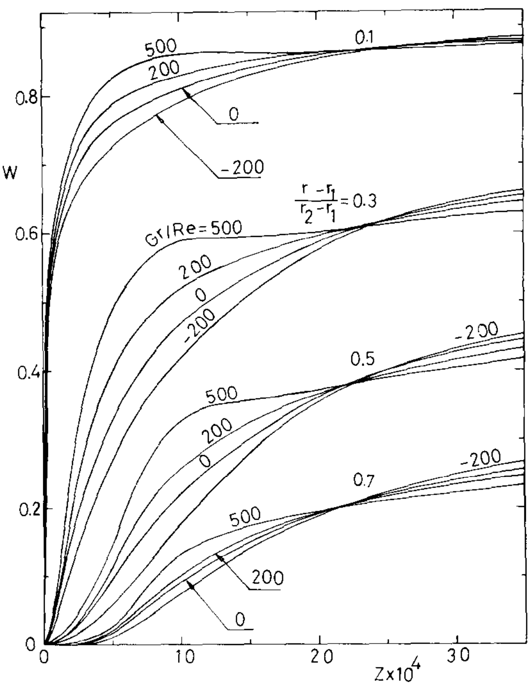

FIG. 4. Tangential velocity development for various values of Gr/Re. $N = 0.9$; $Pr = 0.7$; $Re^2/Ta = 10$; case (O).

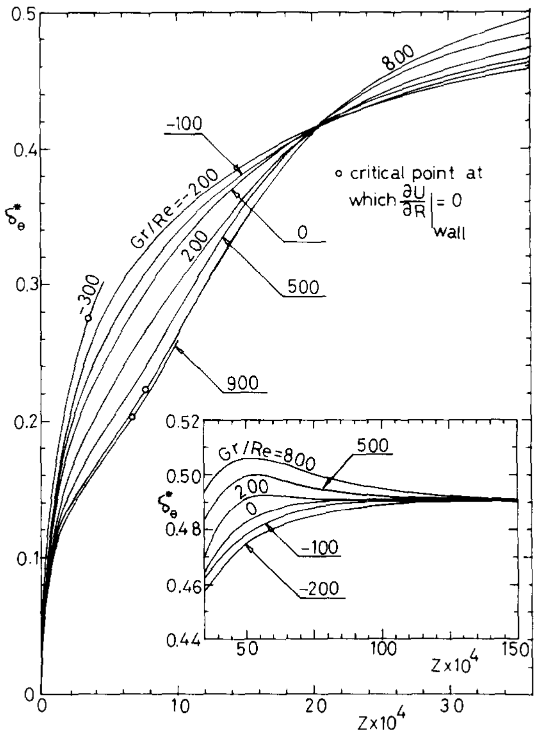

FIG. 6. Tangential boundary layer displacement thickness against axial distance. $N = 0.9$; $Pr = 0.7$; $Re^2/Ta = 10$; case (I).

thermal boundary conditions (O), the radial velocity, near the annulus entrance and until a certain axial distance, mainly transfers fluid from regions close to the rotating inner cylinder to regions far from it, thus causing a transport of tangential momentum from fluid near the inner rotating wall to the core fluid. However, far away from the entrance, the radial velocity mainly transfers fluid of low tangential momentum from regions close to the stationary outer cylinder to the core fluid. On the other hand, for an opposing free convection under thermal boundary conditions (O), the radial velocity component acts in a different manner, i.e. near the annulus entrance, it

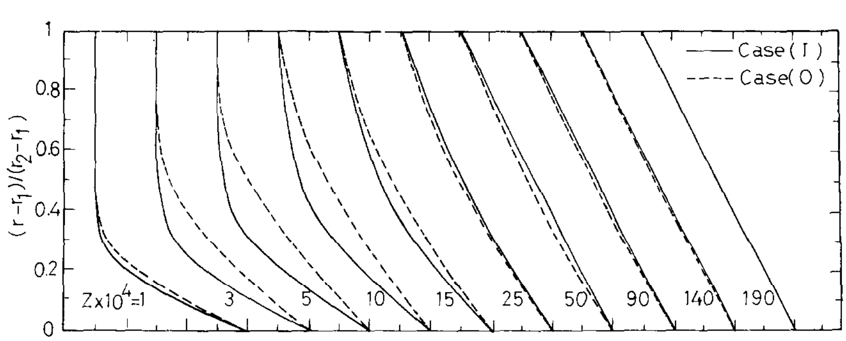

FIG. 5. Effect of thermal boundary conditions on the developing tangential velocity profiles. $N = 0.9$; $Pr = 0.7$; $Re^2/Ta = 10$; $Gr/Re = 500$.

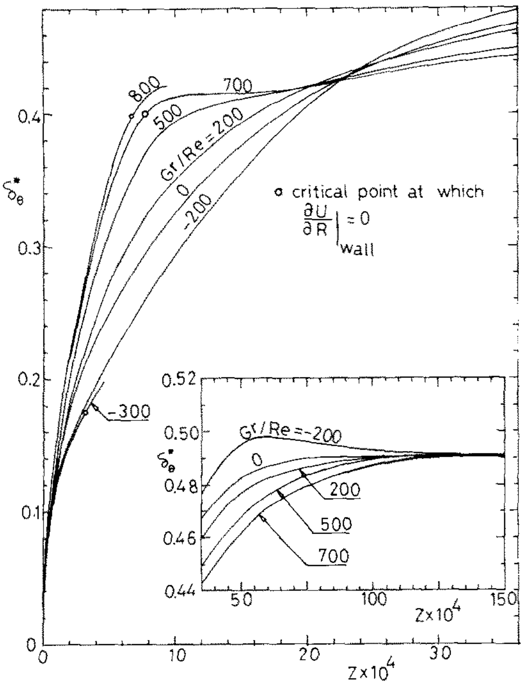

FIG. 7. Effect of superimposed free convection on the dimensionless tangential boundary layer displacement thickness. $N = 0.9$; $Pr = 0.7$; $Re^2/Ta = 10$; case (O).

mainly transfers fluid from regions close to the stationary outer wall but far downstream it mainly transfers fluid, having high tangential momentum, from regions close to the inner rotating wall.

Under thermal boundary conditions (I), the radial velocity component acts, for a given value of the parameter Gr/Re, in a reversed manner compared with that in case (O). To clarify this point, the radial velocity profiles, at a given cross-section in the early stages of development, are drawn in Fig. 9 for various selected values of the parameter Gr/Re. It is clear from this figure that for positive values of Gr/Re (i.e. aiding free convection) the radial velocity component is negative, i.e. its direction is opposite to that of the radial coordinate. However, with negative values of Gr/Re, the radial velocity is positive, i.e. its direction is from the inner rotating wall to the outer stationary wall. Indeed, in the last stages of development (i.e. at large values of Z) the directions of the radial velocity component are opposite to those shown in Fig. 9.

According to Astill's empirical stability criterion for tangentially developing flows [2, 3], the first instability disturbance appears if the Taylor number based on the tangential boundary layer displacement thickness exceeds a certain critical value. Combining this criterion with the present results for δ_θ^*, shown in Figs. 6 and 7, implies that: (1) under thermal conditions (I), a superimposed aiding/opposing free convection tends to stabilize/destabilize a tangentially developing flow in the early stages of development and vice versa in the last stages of development, (2) under thermal boundary conditions (O), a superimposed opposing/aiding free convection respectively stabilizes/destabilizes a tangentially developing laminar flow in the early stages of development but in the last stages of development the reverse is true.

Effect of inner cylinder rotation on laminar mixed convection heat transfer parameters

Table 3 gives the local Nusselt number and the mixing cup temperature for $Pr = 0.7$ at various axial positions from the entrance for an annulus of radius ratio 0.9 under thermal boundary conditions (I) and (O). Under each thermal boundary condition the results are presented, at a selected value of the parameter Gr/Re, for $Re^2/Ta = \infty$ (i.e. the stationary walls case) and $Re^2/Ta = 0.2$ (i.e. the lowest value at which a converged laminar solution could be obtained over the entire development length for the selected value of Gr/Re). In general and as can be seen from these results, the inner cylinder rotation causes, for a given value of Gr/Re, an increase in the local heat transfer coefficient and the mixing cup temperature, if the inner wall is the heated boundary and vice versa if the outer wall is the heated boundary. These effects are attributed to the very same reasons mentioned in [8], i.e. in the entrance region, the inner cylinder rotation causes the axial velocity boundary layer developing on the outer wall to be thickened while the inner wall axial

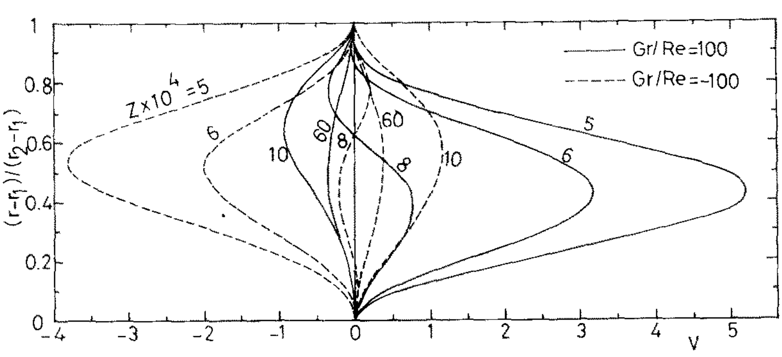

FIG. 8. Effect of free convection on the development of the radial velocity component. $N = 0.9$; $Re^2/Ta = 10$; case (O).

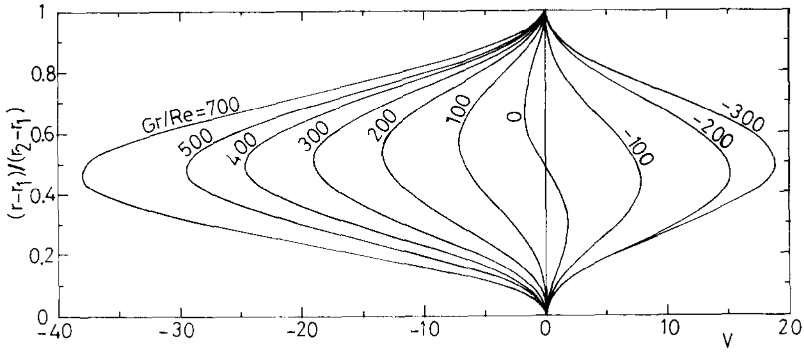

FIG. 9. Effect of the parameter Gr/Re on the radial velocity profiles at $Z = 4 \times 10^{-4}$. $N = 0.9$; $Pr = 0.7$; $Re^2/Ta = 10$; case (I).

Table 3. Effect of the parameter Re^2/Ta on the local Nusselt number and the dimensionless mixing cup temperature, $N = 0.9$, $Pr = 0.7$

	Case (I) with $Gr/Re = 500$				Case (O) with $Gr/Re = -200$			
	Nu		T_m		Nu		T_m	
$Z \times 10^3$	$Re^2/Ta = \infty$	$Re^2/Ta = 0.2$	$Re^2/Ta = \infty$	$Re^2/Ta = 0.2$	$Re^2/Ta = \infty$	$Re^2/Ta = 0.2$	$Re^2/Ta = \infty$	$Re^2/Ta = 0.2$
0.05	12.446	12.952	0.0644	0.0651	8.405	8.214	0.0824	0.0809
0.10	10.112	10.450	0.0988	0.1006	6.788	6.516	0.1083	0.1056
0.30	7.978	8.158	0.1990	0.2028	4.790	4.585	0.1771	0.1740
1.50	6.602	6.991	0.5503	0.5611	4.255	3.998	0.4387	0.4254
4.50	5.363	5.376	0.8630	0.8700	4.564	4.519	0.7918	0.7795
11.50	4.977	4.976	0.9862	0.9867	4.778	4.776	0.9808	0.9781

velocity boundary layer diminishes. However, as can be seen from Table 3, the maximum deviation between the local heat transfer parameters of the stationary walls case and those corresponding to the case of $Re^2/Ta = 0.2$ is about 6%. Therefore, the results presented in [13] for the stationary walls case may be used, without significant errors, for any other value of the parameter Re^2/Ta, provided that the flow remains laminar and the critical distance Z_r, if any, is not reached.

REFERENCES

1. G. I. Taylor, Stability of a viscous liquid contained between two rotating cylinders, *Phil. Trans. R. Soc. Ser.* A, **223**, 289–343 (1923).
2. K. N. Astill, Modes of adiabatic flow in the entrance region of an annulus with an inner rotating cylinder, Ph.D. Dissertation, Massachusetts Institute of Technology (1961).
3. K. N. Astill, Studies of the developing flow between concentric cylinders with the inner cylinder rotating, *J. Heat Transfer* **86**, 383–392 (1964).
4. K. N. Astill, J. T. Ganely and B. W. Martin, The developing tangential velocity profile for axial flow in an annulus with a rotating inner cylinder, *Proc. R. Soc. Lond.* **307A**, 55–69 (1968).
5. B. W. Martin and A. Payne, Tangential flow development for laminar axial flow in an annulus with a rotating inner cylinder, *Proc. R. Soc. Lond.* **328A**, 123–141 (1972).
6. K. C. Chung, The momentum integral solution of the developing flow in the entrance of an annulus with a rotating inner cylinder M.Sc. dissertation, Tufts University, U.S.A. (1973).
7. J. E. R. Coney and M. A. I. El-Shaarawi, A contribution to the numerical solution of developing laminar flow in the entrance region of concentric annuli with rotating inner walls, *J. Fluids Engng* **96**, 333–340 (1974).
8. J. E. R. Coney and M. A. I. El-Shaarawi, Laminar heat transfer in the entrance region of concentric annuli with rotating inner walls, *J. Heat Transfer* **96**, 560–562 (1974).
9. K. M. Becker and J. Kaye, The influence of a radial temperature gradient on the instability of fluid flow in an annulus with an inner rotating cylinder, *J. Heat Transfer* **84**, 106–110 (1962).
10. G. F. Scheele and T. J. Hanratty, Effect of natural convection on stability of flow in a vertical pipe, *J. Fluid Mech.* **14**, 244–256 (1962).
11. L. Lapidus, *Digital Computation for Chemical Engineers*, pp. 254–255. McGraw–Hill (1962).
12. B. Carnahan, H. A. Luther and J. O. Wilkes, *Applied Numerical Methods*, pp. 449–475. John Wiley (1969).
13. M. A. I. El-Shaarawi and A. Sarhan, Free convection effects on the developing laminar flow in vertical concentric annuli, *J. Heat Transfer* **102**, 617–622 (1980).
14. K. C. Chung and K. N. Astill, Hydrodynamic instability of viscous flow between rotating coaxial cylinders with fully developed axial flow, *J. Fluid Mech.* **81**, 641–655 (1977).
15. J. R. Bodoia, Ph.D. thesis, Carnegie Institute of Technology, July 1959.
16. H. Schlichting, Laminar flow about a rotating body of revolution, *NACA TM* 1415 (1956).

CONVECTION MIXTE LAMINAIRE A L'ENTREE D'UN ESPACE ANNULAIRE VERTICAL AVEC CYLINDRE INTERIEUR TOURNANT

Résumé—On présente des résultats numériques d'une méthode aux différences finies pour l'écoulement de couche limite avec convection mixte laminaire dans un espace annulaire vertical avec cylindre interne tournant. On étudie l'effet d'une convection libre favorable ou antagoniste sur les profils de vitesse tangentielle, pour un fluide avec $Pr = 0{,}7$, un espace à rapport de rayons égal à 0,9 et pour les domaines $-300 \leq Gr/Re \leq 800$ et $0{,}2 \leq Re^2/Ta \leq 10$. On considère aussi les effets de la rotation du cylindre intérieur sur la longueur de développement hydrodynamique, sur la distance critique à laquelle le gradient de vitesse axial normal à la paroi s'annule, et sur les paramètres du transfert thermique.

ÜBERLAGERTE ERZWUNGENE UND FREIE KONVEKTION IM EINTRITTSBEREICH EINER VERTIKALEN RINGSPALTSTRÖMUNG MIT ROTIERENDEM INNEREN ZYLINDER

Zusammenfassung—Es wird die numerische Lösung mit Hilfe eines Differenzenverfahrens für eine ausgebildete Überlagerung von erzwungener und freier laminarer Grenzschichtströmung in einem senkrechten Ringspalt mit rotierendem Innenzylinder beschrieben. Der Einfluß einer überlagerten verstärkenden oder hemmenden freien Konvektion im ausgebildeten Geschwindigkeitsprofil wurde für ein Fluid mit $Pr = 0{,}7$ in einem Ringspalt mit dem Radienverhältnis 0,9 über einen Bereich von $-300 \leq Gr/Re \leq 800$ und $0{,}2 \leq Re^2/Ta \leq 10$ untersucht. Die Einflüsse eines rotierenden inneren Zylinders auf die hydraulische Anlauflänge, auf den kritischen Abstand, bei welchem der Gradient der Axialgeschwindigkeit senkrecht zur Wand verschwindet, sowie auf die Wärmeübertragungs-Parameter wurden untersucht.

СМЕШАННАЯ ЛАМИНАРНАЯ КОНВЕКЦИЯ ВО ВХОДНОМ УЧАСТКЕ ВЕРТИКАЛЬНОГО КОЛЬЦЕВОГО КАНАЛА С ВРАЩАЮЩИМСЯ ВНУТРЕННИМ ЦИЛИНДРОМ

Аннотация — Представлены численные результаты конечно-разностным методом для развивающейся смешанной ламинарной конвекции в пограничном слое в вертикальном концентрическом кольцевом канале с вращающимся внутренним цилиндром. Исследуется влияние совпадающей с вынужденным движением или противоположной по направлению конвекции на развивающиеся профили тангенциальной скорости для жидкости с $Pr = 0{,}7$ в кольцевом канале с отношением радиусов 0,9 в диапазоне $-300 \leq Gr/Re \leq 800$ и $0{,}2 \leq Re^2/Ta \leq 10$. Рассматривается влияние вращения внутреннего цилиндра на длину гидродинамического начального участка, а также критическое расстояние, на котором градиент осевой скорости исчезает, и параметры теплообмена.